

# Advanced Topology for Grid-connected Photovoltaic System Based PWM Rectifier

**Abstract.** This paper proposes an advanced topology for grid-connected photovoltaic systems (GCPVS) based on sliding mode control (SMC). The proposed topology exploits the generation and regeneration modes of the three-phase PWM rectifier well suited for high power quality. In addition, it has the advantage of eliminating the inverter and the diode rectifier stages used in the classical structure and replacing them by a PWM rectifier. For maximum power point tracking (MPPT) of the PV generator, DC-Link voltage control and direct power control (DPC), a sliding mode controllers (SMC) are used in order to obtain high accuracy and fast dynamic response against meteorological and load variations. To verify the effectiveness of the control applied on the proposed topology, a wide simulation results are carried out under MATLAB-SIMULINK environment for different operating conditions that confirm the feasibility of the proposed topology.

**Streszczenie.** W artykule zaproponowano zaawansowaną topologię systemów fotowoltaicznych podłączonych do sieci (GCPVS) w oparciu o sterowanie trybem ślizgowym (SMC). Proponowana topologia wykorzystuje tryby generowania i regeneracji trójfazowego prostownika PWM dobrze przystosowanego do wysokiej jakości energii. Dodatkowo ma tę zaletę, że eliminuje stosowane w klasycznej konstrukcji stopnie falownika i prostownika diodowego i zastępuje je prostownikiem PWM. Do śledzenia maksymalnego punktu mocy (MPPT) generatora fotowoltaicznego, sterowania napięciem DC-Link i bezpośredniego sterowania mocą (DPC), stosowane są kontrolery trybu ślizgowego (SMC) w celu uzyskania wysokiej dokładności i szybkiej odpowiedzi dynamicznej na zmiany pogody i obciążenia. Aby zweryfikować skuteczność zastosowanego sterowania na proponowanej topologii, przeprowadza się szerokie wyniki symulacji w środowisku MATLAB-SIMULINK dla różnych warunków pracy, które potwierdzają wykonalność proponowanej topologii. (**Zaawansowana topologia dla podłączonego do sieci systemu fotowoltaicznego prostownika PWM**)

**Keywords:** Sliding Mode Control (SMC), Maximum Power Point Tracking (MPPT), Direct Power Control (DPC), Three Phase PWM.

**Słowa kluczowe:** sterowanie trybem przesuwu (SMC), śledzenie punktu maksymalnej mocy (MPPT), bezpośrednie.

## Introduction

Nowadays, solar energy has become the most important and usable renewable energy in the world due to its multiple benefits, among them: clean, renewable, unlimited and without risk. It can be converted into electrical energy without moving parts [1, 2].

With the increase of fossil fuels cost with their undesirable environmental impacts and due to the fatal decrease of the photovoltaic modules price recently, Photovoltaic (PV) energy production has becomes mature and its participation has expanded in the global energetic mix. As the Grid-connected PV systems topology does not require physical storage systems (batteries,..) that reduce the investment cost, most industrialized countries rely on these renewable systems connected to the electrical grid to cover the lack of energy produced by conventional energy sources [1, 3, 4, 5,6].

Many control techniques have been developed in recent literature and applied on different GCPVS to ensure safe active power injection that is produced by photovoltaic systems with high power quality. This last task is generally done by adding passive or active power filtering systems.

In [7], the authors have proposed an optimal operation of a doubly-stage grid-connected photovoltaic system doted of a shunt active power filter. A fuzzy logic-based maximum power point tracking control is proposed to obtain optimal power delivered by the PV system under different irradiance levels. In the grid side, a predictive direct power control (P-DPC) was used to ensure partial supply of the load with harmonic current compensation.

In reference [8], the authors used the sliding mode control to extract the optimal panel power and the P-DPC technique to ensure both active and reactive power command and power quality control.

Another work presented in [9], relied on a fuzzy logic controller instead of the classical P&O based MPPT in order to overcome the problems related to the sudden and fast variations of the irradiance. On the other hand, the

Synchronous Detection Method (SDM) is used for the identification of harmonic currents.

In 2019, the authors in [10] have adopted another direct topology without adaptation stage. The finite set model predictive technique (FS-MPC) was employed to drive the voltage source inverter (VSI). The cost function is composed of error terms between the injected currents and their references generated by the classical MPPT P&O technique.

In this work, compared to the conventional topology, the proposed configuration consists of replacing the three-phase inverter and the diode rectifier with a PWM rectifier. The load supply is provided by the grid via the PWM rectifier and/or the photovoltaic panel depending on the meteorological conditions of the photovoltaic system. The choice of this topology is justified by its advantages such as the advanced operating characteristics of PWM rectifiers including input sinusoidal current, controllable input power factor, bidirectional power flow, high quality dc output voltage and best efficiency due to reduced commutation and conduction losses. All these advantages lead to an alleviate topology, uncomplicated control and consequently a significant cost reduction.

Given the many advantages of sliding mode technique such as robustness, simplicity of application and fast response, we are interested in the application of this approach for:

- VDC-SMC bus voltage regulation.
- The extraction of the optimal power of the photovoltaic panel MPPT-SMC.
- Direct power control DPC-SMC

## Description of the proposed configuration

The conventional topology for *grid-connected photovoltaic systems (GCPVS)* is depicted by figure1 (a). The PV array supplies the considered load and the excess power is injected in the utility grid according one of many control strategies well explained in previous literature. The overall proposed system configuration is shown in figure 1

(b). It consists of an electrical distribution network having a three-phase balanced voltage source, a three-phase PWM rectifier supplying a load. The PV array is associated with a DC-DC boost converter to participate in feeding the considered load. The boost converter ensures the MPPT functioning and steps up the DC link voltage to an acceptable level which permits a bidirectional flow of the exchanged active and reactive power with the utility grid.

The PWM rectifier is controlled by direct power control strategy based sliding mode control DPC-SMC.

The adopted approach is used in order to manage the exchanged powers of the PV system and the grid according to the climatic conditions of illumination and load variations.

In addition, high power quality such as low current/voltage THD and unity power factor should be guaranteed in the grid side.

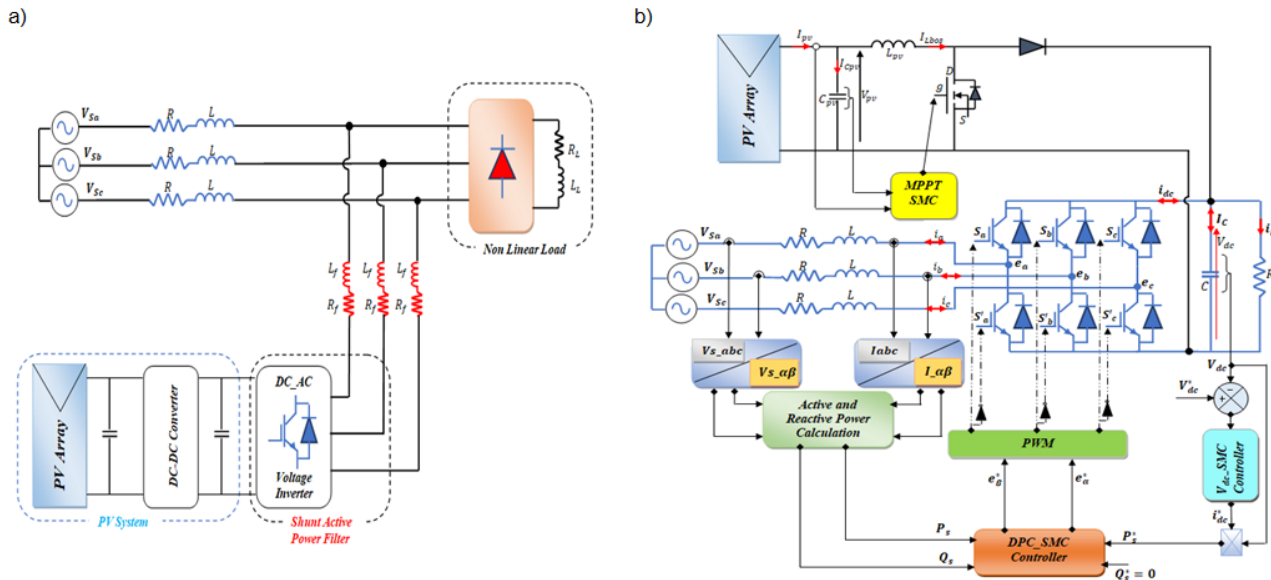


Fig.1. Schematic of the grid-connected PV system: a) the conventional configuration, b) the proposed configuration.

To achieve these objectives, the proposed configuration based on SMC control, is tested by an extensive numerical simulation using Matlab -Simulink. The values of main parameters used are listed in Table 1.

Table1. Electrical parameters system and control coefficients

Line to Line source voltage	$V_S=120V$
System frequency	$F=50Hz$
Line Impedance	$R=0.2\Omega, L=12mH$
Dc-Bus voltage Capacitor	$C_{dc}=2mF$
Dc-Bus voltage reference	$V_{dc}=240V$
Load Resistance	$R_L=40 \Omega$
Boost Input Capacitor	$C_{pv}=2mF$
Boost Inductor	$L_{pv}=0.5mH$
Switching frequency	$F_s=15kHz$
PV Module Power at $1000W/m^2$ (1Soltech 1STH-215-P)	$P_{pv}=213.15W$

The PV array is composed of 2 strings of PV modules connected in parallel. Each string consists of 6 modules of *STH-215-P* of  $213.15 W$  connected in series.

### Control approach

The SMC controllers have attracted more and more attention due to their performances especially for nonlinear systems such as solar energy. Moreover, SMC offers a noteworthy stability and robustness, good dynamic disturbance rejection and fast response [4, 11,12]. For that reasons, three SMC controllers have been designed as cited in the introduction part.

### MPPT based SMC

Figure 2 shows the block diagram of a PV module equipped with an adaptation stage composed of a boost converter used to track efficiently the MPP and to step up the DC-link voltage to an adequate level. The MPPT algorithm is dependent on the type of the chosen implementation and the desired performance. However the

algorithm must adjust the duty cycle ( $D$ ) of the associated power converter according to the output voltage level.

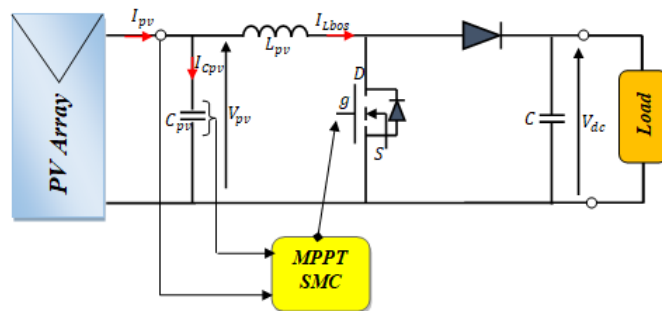


Fig.2. Block diagram of MPPT method.

The mathematical model of the boost converter is given by the equation system (1)

$$(1) \quad \begin{cases} \frac{dV_{pv}}{dt} = \frac{1}{C_{pv}} I_{pv} - \frac{1}{C_{pv}} I_{Lbos} \\ \frac{dI_{Lbos}}{dt} = \frac{1}{L_{pv}} V_{pv} - \frac{1}{L_{pv}} (1 - D) V_{dc} \end{cases}$$

where:  $V_{pv}$ – output voltage of photovoltaic generator,  $I_{pv}$ – output current of photovoltaic generator,  $I_{Lbos}$ – inductor current,  $V_{dc}$ – load voltage,  $D$ – duty cycle.

In order to determine the duty cycle  $D$ , it is necessary to control the current  $I_{Lbos}$ .

According to the first equation of the system (1):

$$(2) \quad \dot{V}_{PV} = \frac{1}{C_{pv}} I_{pv} - \frac{1}{C_{pv}} I_{Lbos}$$

### Sliding surface design

The error  $e_{pv}$  between the output voltage of the photovoltaic panel  $V_{PV}$  and its reference  $V_{PV}^*$  is considered as follows:

$$(3) \quad e_{pv} = V_{PV} - V_{PV}^*$$

The chosen sliding surface  $S_{PV}$  is given by:

$$(4) \quad S_{PV} = e_{PV} = V_{PV} - V_{PV}^*$$

The time derivative  $\dot{S}_{PV}$  of the considered sliding surface  $S_{PV}$  is given as follows:

$$(5) \quad \dot{S}_{PV} = \dot{e}_{PV} = \dot{V}_{PV} - \dot{V}_{PV}^*$$

$$(5) \quad \dot{S}_{PV} = \frac{1}{C_{pv}} I_{pv} - \frac{1}{C_{pv}} I_{Lbos} - \dot{V}_{PV}^*$$

steady state:  $\dot{S}_{PV} = 0$ , leading to:

$$(6) \quad I_{Lbos\_eq} = I_{pv} - C_{pv} \dot{V}_{PV}^*$$

$$I_{Lbos}^* = I_{Lbos\_eq} + I_{Lbos\_DC}$$

where  $I_{Lbos\_eq}$  represents the equivalent term inherent for SMC and  $I_{Lbos\_DC}$  the discontinuous term, then:

$$(7) \quad I_{Lbos}^* = I_{pv} - C_{pv} \dot{V}_{PV}^* + K_{pv} \text{sing}(S_{PV})$$

On the other hand, we use the second equation of the system (1) as:

$$(8) \quad \dot{I}_{Lbos} = \frac{1}{L_{pv}} V_{pv} - \frac{1}{L_{pv}} (1-D)V_{dc}$$

The error  $e_D$  between the inductor current  $I_{Lbos}$  and its reference value  $I_{Lbos}^*$  is considered as follows:

$$(9) \quad e_D = I_{Lbos} - I_{Lbos}^*$$

The chosen sliding surface  $S_D$  is defined as:

$$(10) \quad S_D = e_D = I_{Lbos} - I_{Lbos}^*$$

The time derivative  $\dot{S}_D$  gives:

$$(11) \quad \dot{S}_D = \dot{I}_{Lbos} - \dot{I}_{Lbos}^*$$

by substituting the equations (8) into (11), we find:

$$(12) \quad \dot{S}_D = \frac{1}{L_{pv}} V_{pv} - \frac{1}{L_{pv}} (1-D)V_{dc} - \dot{I}_{Lbos}^*$$

In steady state, the derivative  $\dot{S}_D = 0$ :

$$(13) \quad \frac{1}{L_{pv}} V_{pv} - \frac{1}{L_{pv}} (1-D)V_{dc} - \dot{I}_{Lbos}^* = 0$$

We get:

$$(14) \quad D_{eq}^* = \frac{L_{pv}}{V_{dc}} \dot{I}_{Lbos}^* + 1 - \frac{V_{pv}}{V_{dc}}$$

Then, the duty cycle  $D^*$  is defined by:

$$D^* = D_{eq}^* + D_{DC}^*$$

$$(15) \quad D^* = \frac{L_{pv}}{V_{dc}} \dot{I}_{Lbos}^* - \frac{V_{pv}}{V_{dc}} + 1 + K_D \text{sign}(S_D)$$

### Stability analysis

The candidate Lyapunov function  $V_{PV}$  is given by:

$$(16) \quad \dot{V}_{PV} = S_{PV} \dot{S}_{PV}$$

By replacing equations (5) and (7) into (8), we obtain the equation (17):

$$(17) \quad \dot{V}_{PV} = S_{PV} \left[ \frac{1}{C_{pv}} I_{pv} - \frac{1}{C_{pv}} \left( I_{pv} - C_{pv} \dot{V}_{PV}^* + K_{pv} \text{sing}(S_{PV}) \right) - \dot{V}_{PV}^* \right]$$

After simplification, the equation (17) leads to:

$$(18) \quad \dot{V}_{PV} = -K_{PV} S_{PV} \text{sing}(S_{PV}) = -K_{PV} |S_{PV}| < 0$$

$$\Rightarrow K_{PV} > 0$$

Therefore,  $K_{PV}$  must be a positive constant.

On the other hand, the time derivative of the Lyapunov function  $V_D$  is given by:

$$(19) \quad \dot{V}_D = S_D \dot{S}_D$$

By replacing equations (12) and (15) into (19), we get the equation (20):

$$(20) \quad \dot{V}_D = S_D \left[ \frac{V_{pv}}{L_{pv}} - \frac{V_{dc}}{L_{pv}} + \frac{V_{dc}}{L_{pv}} \left( \frac{L_{pv}}{V_{dc}} \dot{I}_{Lbos}^* - \frac{V_{pv}}{V_{dc}} + 1 + K_D \text{sign}(S_D) \right) - \dot{I}_{Lbos}^* \right]$$

After simplification, the equation (20) is reduced to:

$$(21) \quad \dot{V}_D = K_D S_D \text{sing}(S_D) = K_D |S_D| < 0$$

$$\Rightarrow K_D < 0$$

Therefore,  $K_D$  must be a negative constant.

### Sliding mode DC voltage control

The reference of the grid active power is obtained by the regulation of the DC bus voltage, a good dynamic of this regulation increases the performance of the system.

### Sliding surface design

Several forms of sliding surfaces are proposed in the literature. In our case, we have chosen the following form [14]:

$$(22) \quad S(t) = \left( \lambda + \frac{d}{dt} \right)^{n-1} e(t) + K_1 \int_0^t e(\tau) d\tau$$

Where:  $e(t)$  – the error between the desired and actual values,  $\lambda, K_1$  – are strictly positive constants,  $n$  – is set to 1.

The error  $e_{dc}$  between DC link voltage reference  $V_{dc}^*$  and the actual DC link voltage value  $V_{dc}$  is expressed as follows:

$$(23) \quad e_{dc}(t) = V_{dc}^*(t) - V_{dc}(t)$$

Therefore, the sliding surface  $S_{dc}$  is given by:

$$(24) \quad S_{dc}(t) = e_{dc}(t) + K_1 \int e_{dc}(t) dt$$

The time derivative  $\dot{S}_{dc}$  of the sliding surface  $S_{dc}$  is given by:

$$\dot{S}_{dc} = \dot{e}_{dc} + K_1 e_{dc}$$

$$(25) \quad \dot{S}_{dc} = \dot{V}_{dc}^* + \frac{V_{dc}}{R_L C} + K_1 (V_{dc}^* - V_{dc}) - \frac{1}{C} I_{dc}$$

The main goal of the control is to produce the necessary current  $I_{dc}^*$  in order to force the present voltage  $V_{dc}$  to track perfectly its desired value  $V_{dc}^*$ . The  $I_{dc}^*$  is composed of:

$$(26) \quad I_{dc}^* = I_{dc\_eq} + I_{dc\_DC}$$

In steady state:  $\dot{S}_{dc} = 0$

According to the equation (25), one can get:

$$(27) \quad I_{dc\_eq} = C \dot{V}_{dc}^* + \frac{V_{dc}}{R_L} + K_1 C (V_{dc}^* - V_{dc})$$

$$(28) \quad I_{dc\_DC} = K_{dc} \text{sign}(S_{dc})$$

The sum of the equations (27) and (28) gives:

$$(29) \quad I_{dc}^* = C \dot{V}_{dc}^* + \frac{V_{dc}}{R_L} + K_1 C (V_{dc}^* - V_{dc}) + K_{dc} \text{sign}(S_{dc})$$

Where:  $K_{dc}$  is a constant.

The function  $\text{sign}(S_{dc})$  is defined as:

$$(30) \quad \text{sign}(S_{dc}) = \begin{cases} +1 & \text{if } S_{dc} > 0 \\ -1 & \text{if } S_{dc} < 0 \\ 0 & \text{if } S_{dc} = 0 \end{cases}$$

### Stability analysis

The time derivative of Lyapunov function  $V$  is given by:

$$(31) \quad \dot{V}_{dc} = S_{dc} \dot{S}_{dc}$$

By substituting the equations (25) and (29) into (31), it yields:

$$(32) \quad \dot{V}_{dc} = S_{dc} \left[ \dot{V}_{dc}^* - \frac{1}{C} \left( C \dot{V}_{dc}^* + \frac{V_{dc}}{R_L} + K_1 C (V_{dc}^* - V_{dc}) + K_{dc} \text{sign}(S_{dc}) \right) + \frac{V_{dc}}{R_L C} + K_1 (V_{dc}^* - V_{dc}) \right]$$

After some manipulations, the equation (32) is reduced to:

$$(33) \quad \dot{V}_{dc} = -S_{dc} \frac{K_{dc}}{C} \text{sign}(S_{dc}) = -\frac{K_{dc}}{C} |S_{dc}| < 0 \\ \Rightarrow K_{dc} > 0$$

Therefore,  $K_{dc}$  must be a positive constant.

Finally, the desired active power  $P_S^*$  is calculated as:

$$(34) \quad P_S^* = V_{dc} * I_{dc}^*$$

### Sliding mode direct power control DPC-SMC

In the control scheme shown in Figure 1, the active power reference is provided by the SMC-DC voltage controller given by equation (34). For unity power factor operation, the reactive power reference should be set to zero.

The aim of the control here is to force the active and reactive power to track their required reference values. To do this, an inner loop based on DPC-SMC is used, which provides the appropriate PWM rectifier voltage vector  $[e_\alpha; e_\beta]$  for the pulse width modulation as well as generates the necessary control signals.

The mathematical model of the PWM rectifier in  $(\alpha-\beta)$  coordinates is given by the equation system (35) [14, 15].

$$(35) \quad \begin{cases} L \frac{di_\alpha}{dt} = V_{S\alpha} - e_\alpha - R i_\alpha \\ L \frac{di_\beta}{dt} = V_{S\beta} - e_\beta - R i_\beta \\ C \frac{dV_{dc}}{dt} = S_\alpha i_\alpha + S_\beta i_\beta - \frac{V_{dc}}{R_L} \end{cases} \quad (3)$$

Therefore, the grid active and reactive powers in  $(\alpha-\beta)$  coordinates are given by:

$$(36) \quad \begin{cases} P_S = V_{S\alpha} i_\alpha + V_{S\beta} i_\beta \\ Q_S = V_{S\alpha} i_\beta - V_{S\beta} i_\alpha \end{cases}$$

where:

$V_{S\alpha}; V_{S\beta}; i_{S\alpha}; i_{S\beta}$  – represent respectively grid voltage and current in  $(\alpha-\beta)$  coordinates.

$e_\alpha; e_\beta$  – are the PWM rectifier voltages in  $(\alpha-\beta)$  coordinates.

$V_{dc}; C$  – represent DC bus voltage and DC bus capacitor.

$R_L$  – is the DC load.

$P_S; Q_S$  – Are the grid active and reactive powers.

### Sliding surface design

The error between power and power reference value is considered as follows:

$$(37) \quad e_P(t) = P_S(t) - P_S^*(t)$$

$$(38) \quad e_Q(t) = Q_S(t) - Q_S^*(t)$$

The sliding surfaces of the powers are chosen as:

$$(39) \quad \begin{cases} S_P(t) = e_P(t) + K_3 \int e_P(t) dt \\ S_Q(t) = e_Q(t) + K_4 \int e_Q(t) dt \end{cases}$$

where:  $K_3$  and  $K_4$  are positive integration gains.

In order to obtain the control law, we set the time derivative of the sliding surface to zero:

$$(40) \quad \begin{cases} \dot{S}_P = 0 \\ \dot{S}_Q = 0 \end{cases}$$

By applying this condition, we get:

$$(41) \quad \begin{cases} \dot{S}_P = \dot{e}_P + K_3 e_P = 0 \\ \dot{S}_Q = \dot{e}_Q + K_4 e_Q = 0 \end{cases} \Rightarrow \begin{cases} \dot{e}_P = -K_3 e_P \\ \dot{e}_Q = -K_4 e_Q \end{cases}$$

We substitute the equations (35) and (36) into (41), we find:

$$(42) \quad \dot{S}_P = [\dot{V}_{S\alpha} i_\alpha + \dot{V}_{S\beta} i_\beta + (K_3 - \frac{R}{L}) P_S + \frac{1}{L} (V_{S\alpha}^2 + V_{S\beta}^2) - \dot{P}_S^* - K_3 P_S^*] - \frac{1}{L} (V_{S\alpha} e_\alpha + V_{S\beta} e_\beta)$$

$$(43) \quad \dot{S}_Q = [\dot{V}_{S\beta} i_\alpha - \dot{V}_{S\alpha} i_\beta + (K_4 - \frac{R}{L}) Q_S - \dot{Q}_S^* - K_4 Q_S^*] - \frac{1}{L} (V_{S\beta} e_\alpha - V_{S\alpha} e_\beta)$$

From this analysis, we obtain the control vector  $[e_\alpha; e_\beta]$  by the first time derivative of the sliding surface.

We can rewrite the equations (42), (43) in the following matrix from:

$$(44) \quad \dot{S}_{PQ} = B + A.X$$

where:

$$\dot{S}_{PQ} = \begin{bmatrix} \dot{S}_P \\ \dot{S}_Q \end{bmatrix}$$

$$B = \begin{bmatrix} \dot{V}_{S\alpha} i_\alpha + \dot{V}_{S\beta} i_\beta + (K_3 - \frac{R}{L}) P_S + \frac{1}{L} (V_{S\alpha}^2 + V_{S\beta}^2) - \dot{P}_S^* - K_3 P_S^* \\ \dot{V}_{S\beta} i_\alpha - \dot{V}_{S\alpha} i_\beta + (K_4 - \frac{R}{L}) Q_S - \dot{Q}_S^* - K_4 Q_S^* \end{bmatrix}$$

$$A.X = \frac{1}{L} \underbrace{\begin{bmatrix} -V_{S\alpha} & -V_{S\beta} \\ -V_{S\beta} & V_{S\alpha} \end{bmatrix}}_A \underbrace{\begin{bmatrix} e_\alpha \\ e_\beta \end{bmatrix}}_X$$

In steady state:

$$(45) \quad \dot{S}_{PQ} = 0 \Rightarrow A.X_{eq} = -B$$

$$(46) \quad X_{eq} = -A^{-1}B$$

$$(47) \quad X^* = X_{eq} + X_{DC} = -A^{-1}[B + K_{pq} \text{sing}(S_{PQ})]$$

### Stability Analysis

The time derivative of Lyapunov function  $V_{PQ}$  is given by:

$$(48) \quad \dot{V}_{PQ} = S_{PQ} \dot{S}_{PQ}$$

By replacing the equations (44) and (47) into (48), we obtain the equation (49):

$$(49) \quad \dot{V}_{PQ} = S_{PQ} [A.X + B] \\ \dot{V}_{PQ} = S_{PQ} [A.(-A^{-1}[B + K_{pq} \text{sing}(S_{PQ})]) + B]$$

After simplification, the equation (49) is reduced to:

$$(50) \quad \dot{V}_{PQ} = -K_{pq} S_{PQ} \text{sing}(S_{PQ}) = -K_{pq} |S_{PQ}| < 0 \\ \Rightarrow K_{pq} > 0$$

To satisfy the Lyapunov condition, the factor  $K_{pq}$  must be a positive constant.

### Simulation results

By exploiting the functionality of the PWM rectifier for both generation and regeneration mode and to describe the possible operating conditions of the power system, the power management of the proposed topology is tested for a

variable irradiance profile and load. The two managed modes are:

- ❖  $P_{PV} < P_{Load}$ : The load is supplied by both sources: the grid and the PV panel. In this case, the three PWM rectifier acts in generation mode as a rectifier.
- ❖  $P_{PV} > P_{Load}$ : The load is supplied only by the PV panel and the excess power is injected into the grid which forces the PWM rectifier to operate in regeneration mode as a voltage inverter. The simulation results are shown in Figures 3 to 9.

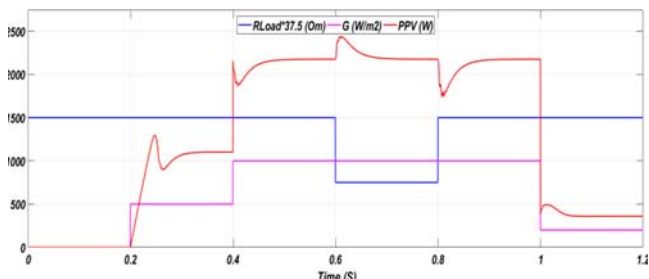


Fig.3. Irradiance profile  $G$ , Variation of the output power  $P_{PV}$  of the PV under load change  $R_{Load}$ .

To test the robustness of the MPPT-SMC algorithm, a variable irradiance profile is established to scan all operating modes of the system. Figure 3, illustrates the irradiance and load profile  $G$ ,  $R_L$  respectively and the generated power  $P_{PV}$  of the PV system.

It can be seen that the evolution of the  $P_{PV}$  output power is in agreement with the applied irradiance profile. For an abrupt and sudden change of illumination in the range [0 – 500 – 1000 – 200  $W/m^2$ ], it is very clear to see that the maximum power point is tracked closely and efficiently and in accordance with the load variations. This result confirms the effectiveness of use of the MPPT SMC strategy in terms of rapid disturbance rejection and fast dynamic response.

Figure 4 shows the behavior of the DC-link voltage where it correctly tracks its reference (240V) in a few milliseconds with negligible tracking error (less than 4%) and minimum overshoots and undershoots even when the load and irradiance change. This good disturbance rejection obtained proves the efficacy and the robustness of the used SMC controller which has a large impact on the active power response as shown in figure 5.

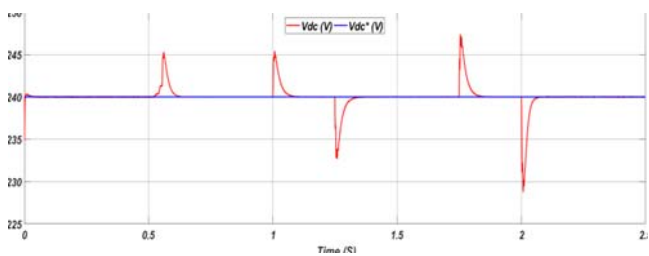


Fig.4. Output dc link voltage regulation under load and irradiance change.

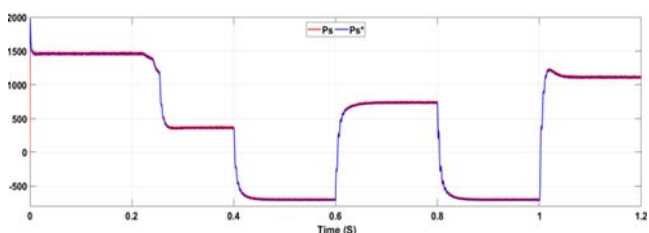


Fig.5. Grid active power and its reference.

Figure 6 shows the evolution of the different active powers, namely: grid active power  $P_s$ , load active power

$P_{Load}$  and generated photovoltaic power  $P_{PV}$  for a variable irradiance profile given in the previous section.

In figure 6, the grid active power  $P_s$  follows correctly the trajectory imposed by the control:

Between 0s to 0.2s the active power  $P_{PV}$  generated by the PV system is zero (zero irradiance), the electrical network provides all the active power required by the load and the PWM rectifier operates in generation mode.

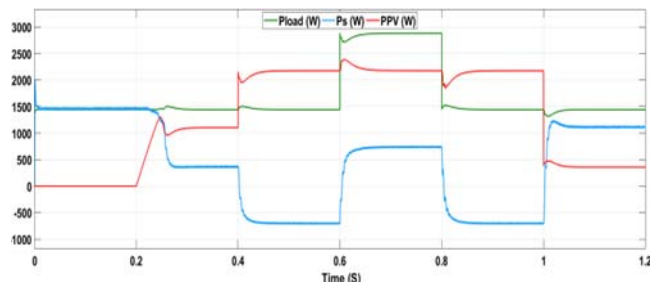


Fig.6. Variation of grid active power  $P_s$ , Load active power  $P_{Load}$  and active power of PV system  $P_{PV}$  under Load and Irradiance change

in the interval [0.2s to 0.4s], the irradiance level  $G$  is increased promptly to  $500W/m^2$ , the  $P_{PV}$  still less than the load active power  $P_{Load}$  ( $P_{PV} < P_{Load}$ ), the two generators contribute simultaneously to supply the load resulting in a decrease of the grid current which stays in phase with the grid voltage as shown in figure 7.2.

In the range [0.4s to 0.6s], the irradiance level  $G$  is increased suddenly again and becomes  $1000W/m^2$ . The  $P_{PV}$  value is greater than the load power  $P_{Load}$  ( $P_{PV} > P_{Load}$ ), in this case, the grid active power  $P_s$  takes a negative value and the PWM rectifier operates in regeneration mode. Indeed, the grid voltage and current become in opposite phase as shown by figure 7.3. The phase shift proves that the grid receives the active power generated by the PV system after subtracting the power consumed by the load.

Between [0.6s to 0.8s], the load is stepped down from  $40\Omega$  to  $20\Omega$ . It can be seen that the  $P_{PV}$  active power keeps its value with negligible overshoot and undershoot. The grid active power changes its direction and takes a positive values meaning that the PWM rectifier operates in generator mode.

In the range [0.8s to 1s], the system backs to the previous state, where the load resistance takes its initial value ( $R_L = 40\Omega$ ), the same observations are also remarked as in the interval [0.4s to 0.6s].

In the last part of the studied cycle [1s - 1.2s], an abrupt decrease of irradiance ( $200W/m^2$ ) is applied, the same remarks made for the interval [0.2s - 0.4s] stay valid except that for the grid current which increases as shown in Figure 7.5.

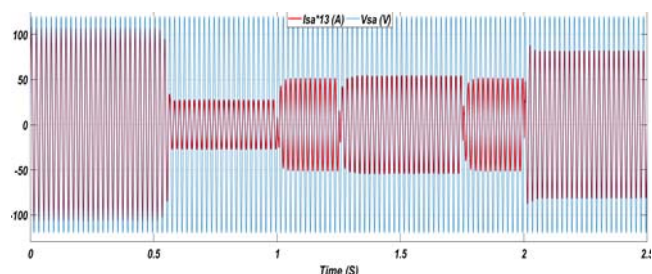


Fig.7. Variations of grid voltage and current under Load and Irradiance change.

Figure 7 shows the evolution of the grid current versus its voltage. It can be seen that the current profile follows the variation of the illumination imposed on the system, reflecting on the behavior of the current in face to the grid

voltage, sometimes in phase when the grid generates its power and sometimes in opposite phase when the grid receives the excess power from the PV system.

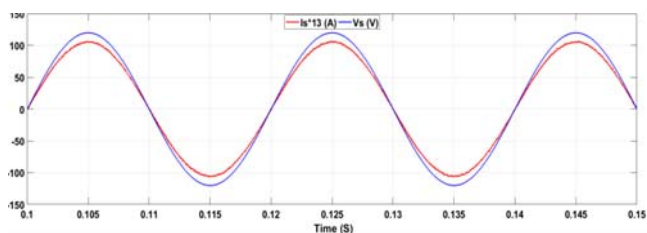


Figure 7.1 Zoom of Grid Voltage and Current during [0s to 0.2s].

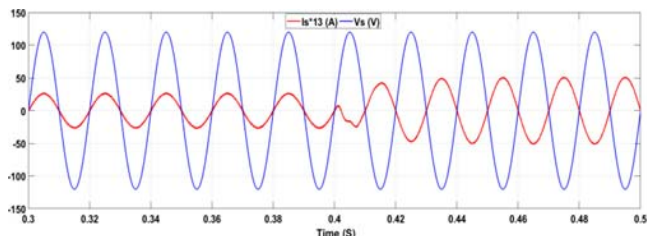


Fig.7.2. Zoom of grid voltage and current during [0.2s to 0.6s].

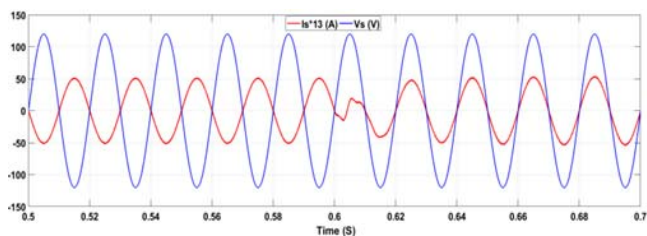


Fig. 7.3 Zoom of grid voltage and current during [0.4s to 0.8s].

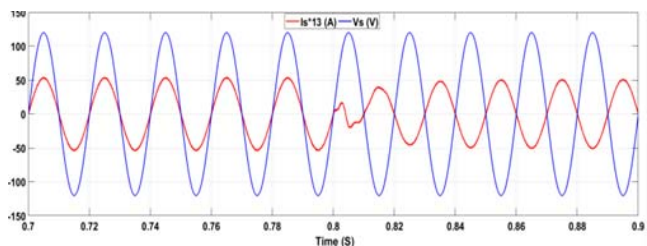


Fig.7.4 Zoom of grid voltage and current during [0.6s to 1s].

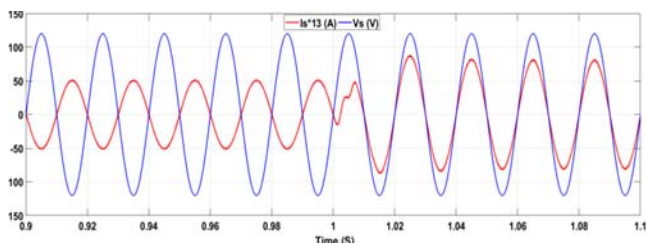


Fig. 7.5 Zoom of grid voltage and current during [0.8s to 1.2s].

One of the main objectives of the present work is to ensure a high power quality in the grid side by minimizing the total harmonic distortion that must be lower than 5%.

Figure 8 shows the curve of the balanced three phase current system associated with the numerical values of the THD for different time ranges. The results are satisfactory and values are in accordance with international standards.

Figure 9 shows the grid active and reactive power shapes and their references. It can be seen that the reactive power is maintained at zero, meanwhile the active power follows perfectly and stably the trajectory imposed by its reference.

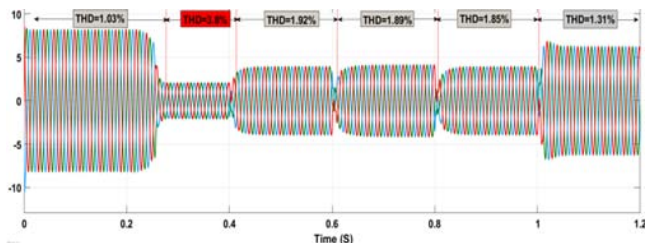


Fig.8. Grid currents and their total harmonic distortion for each operation mode.

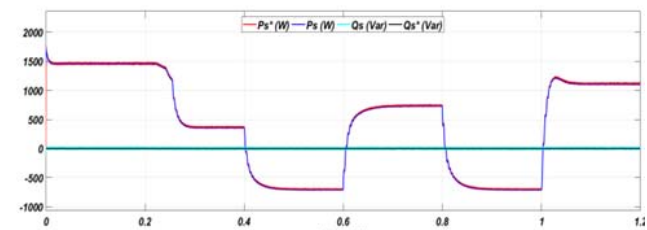


Fig.9. Grid active and reactive powers.

As a result, the application of the DPC-SMC technique on the proposed configuration is able to reduce the currents THD, compensates the reactive power consumed by the load, and injects the excess active power of the GPV into the grid. These functions allow the proposed topology to operate at unity power factor.

## Conclusion

This work presents a design procedure of a grid-connected PV system based on a PWM rectifier well suited for such application. For the proposed topology, a control system based on sliding mode control is performed for both DC bus voltage regulation, MPPT maximum power point tracking and active and reactive power control. Such a control based SMC allowed us to optimize the power flow management between the grid, the PV system and the load. Several objectives and good results have been achieved such as system flexibility, high power quality of the grid with unity power factor, low harmonic distortion rate, robustness of the control against disturbances thanks to the inherent properties of the SMC. The high performance obtained by simulation demonstrates that the proposed topology associated to SMC control is a good alternative for grid-connected PV systems.

## REFERENCES

- [1] Yang B., Li W., Zhao Y., and He X., "Design and analysis of a grid-connected photovoltaic power system," *IEEE Transactions on Power Electronics*, vol. 25, no. 4, 2010.
- [2] Fei W., Duarte J. L., and Hendrix M. A. M., "Grid-interfacing converter systems with enhanced voltage quality for microgrid application-concept and implementation," *IEEE Transaction on Power Electronics*, vol. 26, no. 12, pp. 3501–3513, December 2011.
- [3] Serkan Sezen., Ahmet Aktas., Mehmet Ucar., and Engin Ozdemir, "A Three-Phase Three-Level NPC Inverter Based Grid-Connected Photovoltaic System With Active Power Filtering," *16th International Power Electronics and Motion Control Conference and Exposition*. Antalya, Turkey 21-24 Sept 2014.
- [4] Menadi A., Abdeddaim S., Ghamri A., and Betka, A., "Implementation of fuzzysliding mode based control of a grid connected photovoltaic system," *ISA Transaction*. 58, 586–594. 0019-0578/& Published by Elsevier Ltd. on behalf of ISA. 2015.
- [5] Neves F., Carrasco M., Mancilla-David F., Azevedo G., and Santos V., "Unbalanced grid fault ride-through control for single-stage photovoltaic inverters. *IEEE Transaction on Power Electronics*. 2015. 31, 1.
- [6] Shi J., Zhang W., Zhang Y., Xue F., and Yang T., "MPPT for PV systems based on a dormant PSO algorithm," *Electr. Power Syst*, 2015. Res. 123, 100–107.

- [7] Ouchen S., S Abdeddaim., Betka A., and Menadi A, "Fuzzy-predictive direct power control implementation of a grid connected photovoltaic system, associated with an active power filter," *Energy Conversion and Management*. Volume 122, 15 August 2016, Pages 515-525.
- [8] Ouchen S., S Abdeddaim., Betka A., and Menadi A, "Experimental validation of sliding mode-predictive direct power control of a grid connected photovoltaic system, feeding a nonlinear load," *Solar Energy*. Volume 137, 1 November 2016, Pages 328-336.
- [9] Mouna Tali., Ahmed Esadki., Tamou Nasser., and Boualem Boukezata, "Active Power Filter for Power Quality in Grid Connected PV-System using an Improved Fuzzy Logic Control MPPT," 6th International Renewable and Sustainable Energy Conference (IRSEC). 2018.
- [10] Erdal Irmak., and Naki Güler, "A model predictive control based hybrid MPPT method for boost converters," *International Journal of Electronics*. Vol 107, 2020.
- [11] Montoya D.G., Ramos-Paja C.A., and Giral R, "Improved design of sliding-mode controllers based on the requirements of MPPT techniques. *IEEE Trans. Power Electron*. 31, 235–247. 2016.
- [12] Chu C.-C., and Chen C.-L, "Robust maximum power point tracking method for photovoltaic cells: a sliding mode control approach," *Sol. Energy* 83, 1370–1378, 2009.
- [13] Sumukh Surya., and M. N. Arjun, "Mathematical Modeling of Power Electronic Converters," *SN Computer Science* (2021) 2:267, Springer Nature.
- [14] Barkat S., Tlemçani A., and Nouri H, "Direct power control of the PWM rectifier using sliding mode control," *International Journal of power and energy conversion*, Vol. 2, No. 4. January 2011.
- [15] Bouafia A., Gaubert J.-P., and Krim F, "Design and implementation of predictive current control of three-phase PWM rectifier using space-vector modulation (SVM)". *Energy Convers. Manage.* 2010. 51, 2473–2481.